Simulation of Fluid–Particles Flows: Heavy Particles, Flowing Regime and Asymptotic-Preserving Schemes

Thierry Goudon*†, Shi Jin and Bokai Yan‡

February 3, 2011

Abstract

We are interested in an Eulerian–Lagrangian model describing particulate flows. The model under study consists of the Euler system and a Vlasov-Fokker-Planck equation coupled through momentum and energy exchanges. This problem contains asymptotic regimes that make the coupling terms stiff, and lead to a limiting model of purely hydrodynamic type. We design a numerical scheme which is able to capture this asymptotic behavior, without requiring prohibitive stability conditions. The construction of this Asymptotic Preserving scheme relies on an implicit discretization of the stiff terms which can be treated by efficient inversion methods. This method is a natural coupling of a kinetic solver for the particles with a kinetic scheme for the hydrodynamic Euler equations. Numerical experiments are conducted to study the performance of this scheme in various asymptotic regimes.

Key words. Fluid–particles flows. Hydrodynamic regimes. Asymptotic Preserving schemes. Kinetic schemes.

2010 MSC Subject Classification. 82C80 82C40 35L65 35Q35 65M06 76N15 76M20

1 Introduction

This paper is devoted to the numerical simulation of certain two-phase flows, where a disperse phase, which is a large set of "particles" that could be bubbles, droplets, dusts..., interacts with a dense phase, the surrounding fluid. There are many possible models for such flows. The microscopic models are based on fluid equations defined on disjoint domains and coupled by time-varying interface boundary conditions. The macroscopic (or "Eulerian–Eulerian") models are based on coupled fluid equations describing both phases and defined on a common domain, and these models involve volume fraction and non-conservative terms [30]. The mesoscopic models consist of coupled fluid and kinetic equations. We refer for instance to the overview [19] for a presentation of the different approaches. In what follows we are concerned with the so-called "Eulerian-Lagrangian" framework, or "mesoscopic" description where we adopt a statistical viewpoint for the disperse phase. It means that the set of particles is described through a particle distribution function in phase space $f(t,x,v)$: the integral

$$\int_\Omega f(t,x,v)\,\mathrm{d}v\,\mathrm{d}x$$

*Project-Team SIMPAF, INRIA Lille Nord Europe Research Centre, Park Plazza, 40 avenue Halley, 59650 Villeneuve d'Ascq cedex

†Labo P. Painlevé UMR 8524 CNRS & Université des Sciences et Technologies Lille 1

‡Department of Mathematics University of Wisconsin–Madison, 480 Lincoln Drive, Madison, WI 53706, USA

represents the number of particles occupying at time t the volume $\Omega \subset \mathbb{R}^N \times \mathbb{R}^N$ of the phase space, x being the position variable and v the velocity variable. The particle distribution function can be assocaited with the macroscopic quantities– those observable by experiments–by taking the moments:

$$\begin{cases} \text{the macroscopic density:} & n(t,x) = \displaystyle\int_{\mathbb{R}^N} f(t,x,v)\,\mathrm{d}v, \\ \text{the momentum:} & nV(t,x) = \displaystyle\int_{\mathbb{R}^N} v\ f(t,x,v)\,\mathrm{d}v, \\ \text{the total energy:} & E_P = \frac{1}{2}n|V|^2(t,x) + \frac{1}{2}NnΘ_P = \displaystyle\int_{\mathbb{R}^N} \frac{1}{2}|v|^2\ f(t,x,v)\,\mathrm{d}v, \\ \text{the heat flux:} & q(t,x) = \displaystyle\int_{\mathbb{R}^N} v\ \frac{|v|^2}{2}\ f(t,x,v)\,\mathrm{d}v. \end{cases}$$

Here V is the averaged particle velocity, and Θ_P the temperature of particles. The fluid is described by its density $\rho(t,x) \geq 0$, its velocity $u(t,x) \in \mathbb{R}^N$ and its total energy $E(t,x) \geq 0$. For further purposes, we introduce the internal energy e, the pressure p, the temperature Θ defined by the relations

$$e = \frac{p}{(\gamma-1)\rho} \geq 0, \qquad p = \rho\Theta, \qquad E = e + \frac{u^2}{2}$$

where $1 < \gamma \leq (N+2)/N$ is the adiabatic constant.

According to the hierarchy introduced by O'Rourke [40], we are interested in the so–called "Thin Sprays" where the two phases interact through momentum and energy exchanges, but the effect due to the volume fraction of the particles is neglected. The leading effect that couples the evolution of the disperse and dense phases is due to drag forces. In the system of PDEs we need to introduce a few more physical quantities:

- $\rho_P > 0$ and $\rho_F > 0$ stand for the typical densities of the particles and of the fluid, respectively.
- Both phases are subject to an external potential Φ which deviates the trajectories of the particles. The (real–valued) coefficients η_F and η_P account for the fact that the external potential can act differently, both in orientation and amplitude, on the two phases. A typical example is given by gravity/buoyancy forces. In this case $\nabla_x\Phi = ge_z$, with e_z the unit downward vector, g is the gravitational acceleration, and we set $\eta_F = 1$, $\eta_P = (1 - \rho_F/\rho_P)$. Other relevant examples are given by centrifugal forces or electric forces when considering charged particles immersed in a neutral fluid.
- The Stokes number $\varepsilon > 0$ is the ratio of the Stokes settling time (that is $\frac{2\rho_P a^2}{9\mu}$, with μ the dynamic viscosity of the fluid and a the typical radius of the particles) over a certain time unit of observation. It characterizes the strength of the drag exerted by the fluid on the particles.

We refer to [5, 7, 12, 13, 36] for thorough discussions on the modeling issues. In dimensionless form the equations which govern the system read as follows: the evolution of the density f is determined by Fokker-Planck equation

$$\partial_t f + v\cdot\nabla_x f = \frac{1}{\varepsilon}L_{u,\Theta}f + \eta_P\nabla_x\Phi\cdot\nabla_v f \tag{1}$$

where the Fokker-Planck operator

$$L_{u,\Theta}f = \mathrm{div}_v\big((v-u)f + \Theta\nabla_v f\big), \tag{2}$$

while the evolution of the fluid obeys the Euler system

$$\begin{cases} \partial_t\rho + \mathrm{div}_x(\rho u) = 0, \\ \partial_t(\rho u) + \mathrm{Div}_x(\rho u\otimes u) + \nabla_x p = \dfrac{1}{\varepsilon}\dfrac{\rho_P}{\rho_F}\mathscr{F} - \eta_F\rho\nabla_x\Phi, \\ \partial_t(\rho E) + \mathrm{div}_x\big((\rho E + p)u\big) = \dfrac{1}{\varepsilon}\dfrac{\rho_P}{\rho_F}\mathscr{E} - \eta_F\rho u\cdot\nabla_x\Phi. \end{cases} \tag{3}$$

The Fokker-Planck operator $L_{u,\Theta}$ in (2) describes the following physical effects the particles are subject to due to their environment:

- The drag force exerted by the surrounding fluid is supposed to be proportional to the relative velocity $(v-u)$,
- Diffusion with respect to the velocity variable arises due to the Brownian motion, which involves the temperature Θ of the fluid, [20, 21].

Many additional effects are simply disregarded, such as the added mass effect, the interparticles collisions, or size variations due to coagulation and fragmentation phenomena. Note that the viscosity of the fluid enters in the definition of the parameter ε while viscous effects are neglected on the evolution of the fluid. This can be justified, at least formally, by suitable scaling arguments. The disperse phase influences the dense phase through the coupling terms $\mathscr{F}$ and $\mathscr{E}$. They are defined by

$$\begin{aligned}
&\text{Momentum Exchanges:} \qquad \mathscr{F} &&= -\int_{\mathbb{R}^N} v\, L_{u,\Theta} f \,\mathrm{d}v = \int_{\mathbb{R}^N} (v-u) f \,\mathrm{d}v = n(V-u),\\
&\text{Energy Exchanges:} \qquad \mathscr{E} &&= -\int_{\mathbb{R}^N} \frac{v^2}{2}\, L_{u,\Theta} f \,\mathrm{d}v = \int_{\mathbb{R}^N} (v(v-u) - N\Theta) f \,\mathrm{d}v\\
& &&= n(V-u)\cdot u + Nn(\Theta_P - \Theta) + n|V-u|^2\\
& &&= n(V-u)\cdot V + Nn(\Theta_P - \Theta).
\end{aligned} \tag{4}$$

The definition of the coupling terms $\mathscr{F}$ and $\mathscr{E}$ induces conservation properties. Let us write the system satisfied by the moments of f, that is

$$\begin{aligned}
&\partial_t n + \mathrm{div}_x(nV) = 0,\\
&\partial_t(nV) + \mathrm{Div}_x \mathbb{P} + \eta_P n \nabla_x \Phi = -\frac{1}{\varepsilon} n(V-u)\\
&\partial_t \Upsilon + \mathrm{div}_x q + \eta_P nV\cdot\nabla_x\Phi = -\frac{1}{\varepsilon}\big(n(V-u)\cdot V + Nn(\Theta_P-\Theta)\big) = -\frac{1}{\varepsilon}\big(2\Upsilon - nV\cdot u - Nn\Theta\big),
\end{aligned}$$

with $\Upsilon = (nV^2 + Nn\Theta_P)/2$ and $\mathbb{P} = \int_{\mathbb{R}^N} v\otimes v f \,\mathrm{d}v$. Combined with the fluid equations, it leads to the following conservation laws

$$\begin{aligned}
&\partial_t\Big(\rho u + \frac{\rho_P}{\rho_F} nV\Big) + \mathrm{Div}\Big(\rho u\otimes u + p + \frac{\rho_P}{\rho_F}\mathbb{P}\Big) + \Big(\eta_F\rho + \eta_P\frac{\rho_P}{\rho_F} n\Big)\nabla_x\Phi = 0,\\
&\partial_t\Big(\rho E + \frac{\rho_P}{\rho_F}\Upsilon\Big) + \mathrm{div}\Big((\rho E + p)u + \frac{\rho_P}{\rho_F} q\Big) + \Big(\eta_F\rho u + \eta_P\frac{\rho_P}{\rho_F} nV\Big)\cdot\nabla_x\Phi = 0.
\end{aligned} \tag{5}$$

The total momentum and the total energy are conserved.

Besides the conservation of total momentum and energy, another key feature of the model is the dissipation properties that we describe now. To this end, set the "local Maxwellian"

$$M_{u,\Theta}(v) = (2\pi\Theta)^{-N/2}\exp\Big(-\frac{|v-u|^2}{2\Theta}\Big).$$

The crucial observation consists in rewriting

$$L_{u,\Theta} f = \Theta\ \mathrm{div}_v\Big(M_{u,\Theta}\nabla_v\Big(\frac{f}{M_{u,\Theta}}\Big)\Big).$$

We consider the fluid–entropy $S(t,x)$ defined by the relation

$$S = -\frac{1}{\gamma-1}\ln\big(p\rho^{-\gamma}\big) = -\frac{1}{\gamma-1}\ln\Big(\frac{\Theta}{\rho^{\gamma-1}}\Big).$$

Then, as already remarked in [5], the total energy is conserved and the total entropy is dissipated since

$$\frac{\mathrm{d}}{\mathrm{d}t}\Big(\rho_F\int_{\mathbb{R}^N}\rho E\,\mathrm{d}x+\rho_P\int_{\mathbb{R}^N}\int_{\mathbb{R}^N}\frac{v^2}{2}\,f\,\mathrm{d}v\,\mathrm{d}x+\eta_P\rho_P\int_{\mathbb{R}^N}\int_{\mathbb{R}^N}f\Phi\,\mathrm{d}v\,\mathrm{d}x+\eta_F\rho_F\int_{\mathbb{R}^N}\rho\Phi\,\mathrm{d}x\Big)=0, \tag{6}$$

and

$$\begin{aligned}&\frac{\mathrm{d}}{\mathrm{d}t}\Big(\rho_F\int_{\mathbb{R}^N}\rho S\,\mathrm{d}x+\rho_P\int_{\mathbb{R}^N}\int_{\mathbb{R}^N}f\ln(f)\,\mathrm{d}v\,\mathrm{d}x\Big)\\&=-\frac{\rho_P}{\varepsilon}\left(\int_{\mathbb{R}^N}\int_{\mathbb{R}^N}\Big|\sqrt{\Theta}\frac{\nabla_v f}{\sqrt{f}}+\frac{v-V}{\sqrt{\Theta}}\sqrt{f}\Big|^2\,\mathrm{d}v\,\mathrm{d}x+\int_{\mathbb{R}^N}\int_{\mathbb{R}^N}f\frac{|V-u|^2}{\Theta}\,\mathrm{d}v\,\mathrm{d}x\right)\le 0.\end{aligned} \tag{7}$$

Here the problem is defined in the whole space, but similar manipulations hold when considering standard reflection laws for the particles and boundary conditions for the fluid, see [12]. Note that the dissipation terms in (7) vanish when

$$u=V\quad\text{ and }\quad f(t,x,v)=\frac{n(t,x)}{\big(2\pi\Theta(t,x)\big)^{N/2}}\,\exp\Big(-\frac{|v-V(t,x)|^2}{2\Theta(t,x)}\Big).$$

For such an equilibrium, the temperatures of the two phases equilibrate $\Theta=\Theta_P$ and they have a common macroscopic velocity.

We are interested in the situation where the parameter ε can become small. In this regime, the conservation and dissipation properties detailed above are the basis to describe the asymptotic behavior of the model. In the next Section we shall describe on formal grounds the asymptotic behavior of the solutions for $\varepsilon << 1$. In this regime, the operator $L_{u,\Theta}$ and the coupling terms are stiff, and one can expect the relaxation effect that prescribes the form of the particles distribution function, and as a consequence, one arrives at a set of macroscopic equations to describe the particles–fluid mixture. In Section 3 we design a numerical scheme able to treat the stiffness of the problem efficiently. This scheme belongs to the class of the so-called Asymptotic-Preserving (AP) schemes because it is able to capture the correct asymptotic behavior without suffering the prohibitive scaling-parameter-dependent numerical constraints, see [31] and for a recent overview [24]. In order to define a scheme for the coupled system we find it convenient to discretize the Euler equations by using the Kinetic Schemes [15, 16, 17, 42, 43, 44]. We finally conduct numerical simulations in Section 4, and numercially study some relevant variations of the model.

2 The Hydrodynamic Regimes

For equation (1), as $\varepsilon\to 0$, the Fokker-Planck operator vanishes, which yields

$$f(t,x,v)\simeq\frac{n(t,x)}{(2\pi\Theta)^{N/2}}\exp\Big(-\frac{|v-u(t,x)|^2}{2\Theta(t,x)}\Big). \tag{8}$$

This ansatz is in agreement with the dissipation estimate (7). One can now find the limiting equations satisfied by ρ,u,Θ, and n. To this end we go back to the conservation laws (5). The ansatz (8) yields $nV\simeq nu$, $\Theta_P\simeq\Theta$, $\mathbb{P}\simeq nu\otimes u+n\Theta\mathbb{I}$, and $q\simeq(nu^2+(N+2)n\Theta)/2$. Therefore one arrives at the following limit system

$$\begin{aligned}&\partial_t\rho+\mathrm{div}_x(\rho u)=0,\\&\partial_t n+\mathrm{div}_x(nu)=0,\\&\partial_t\Big(\Big(\rho+\frac{\rho_P}{\rho_F}n\Big)u\Big)+\mathrm{Div}_x\Big(\Big(\rho+\frac{\rho_P}{\rho_F}n\Big)u\otimes u+p+\frac{\rho_P}{\rho_F}n\Theta\Big)+\Big(\eta_F\rho+\eta_P\frac{\rho_P}{\rho_F}n\Big)\nabla_x\Phi=0,\\&\partial_t\Big(\Big(\rho+\frac{\rho_P}{\rho_F}n\Big)\frac{u^2}{2}+\frac{\rho\Theta}{\gamma-1}+\frac{\rho_P}{\rho_F}\frac{N}{2}n\Theta\Big)\\&\qquad+\mathrm{div}_x\Big(\Big[\Big(\rho+\frac{\rho_P}{\rho_F}n\Big)\frac{u^2}{2}+\frac{\gamma}{\gamma-1}\rho\Theta+\frac{\rho_P}{\rho_F}\frac{N+2}{2}n\Theta\Big]u\Big)+\Big(\eta_F\rho+\eta_P\frac{\rho_P}{\rho_F}n\Big)u\cdot\nabla_x\Phi=0.\end{aligned} \tag{9}$$

The system can be seen as the Euler system for the composite density $\rho + \frac{\rho_P}{\rho_F} n$, the composite pressure $\big(\frac{\gamma}{\gamma-1}\rho + \frac{N+2}{2}\frac{\rho_P}{\rho_F} n\big)\Theta$ and the common velocity u and temperature Θ, plus an additional mass conservation equation for ρ (or n).

The mathematical analysis of such fluid–kinetic systems is highly challenging. The difficulty lies on the nonlinear coupling of PDEs of different nature. Different models for the fluid (compressible or incompressible, viscous or inviscid...) introduce different levels of difficulty. A first attempt was to prove the local existence of smooth solutions, see [3, 36] for the analysis of the Euler-Vlasov systems. Another approach concerning classical solutions restricts to solutions close to the equilibrium, by using perturbation techniques and energy estimates [28, 11]. The global existence of weak solutions has been investigated, mainly considering viscous flows, by using fixed point and/or compactness arguments. A crucial step of these proofs relies on the construction of suitable approximations preserving the dissipation properties of the system [29, 37, 38, 6]. Identification of relevant scaling and discussion of asymptotic problems appeared in [10, 26, 27, 38, 12, 5, 36], see also [14] for the analysis of fine properties of the limit hydrodynamic systems. These problems are motivated by combustion theory [40, 49] with applications for the design of performing engines [22] or rocket propulsors [35]. The equations also arise in the modeling of atmospheric pollution [46, 48], sedimentation processes [4, 8], rain formation [23] or dispersion of volcanic columns [41]. It is also worth mentioning the applications in the description of biomedical sprays [2, 39]. In what follows, we are concerned with the design of an efficient numerical scheme, specifically suitable for the asymptotic regime of small ε's in (1)–(3).

3 An AP Scheme for the Flowing Regime

A standard numerical scheme for the system (1)–(3) faces some difficulties, and becomes inefficient in the regime $0 < \varepsilon \ll 1$. The main numerical issues include:

a) The presence of stiff terms lead to the increase of computational cost due to numerical stability constraints;

b) The scheme is required to recover as ε goes to the 0 the behavior of the solutions of the limit equations (9) with ε-independent mesh sizes and time steps;

c) The system couples a kinetic and a hydrodynamic equations;

c) The system has remarkable conservation and dissipation properties that, ideally, should be preserved at the discrete level.

These questions are already addressed in [13], for isentropic flows, where splitting methods are introduced: the kinetic equation is solved first, the hydrodynamic fields being fixed during this time step; then, (ρ, u, Θ) are updated by using an anti-diffusive scheme for the Euler system, see [18, 33, 34], with source terms defined with the new values of the particles distribution function. This strategy is very efficient when dealing with another scaling – the so-called "Bubbling Regime" —- of the equation which yields a diffusion equation for the particles density, see also [7] for the discussion of energy exchanges. In [13] the splitting method has been adapted to the present scaling. Here we propose a different approach to treat the Flowing regime: the method we propose combines the AP approach and kinetic schemes for the hydrodynamic equations. It contains a very efficient implementation of the implicit stiff terms, and with the desired AP properties in the flowing regimes.

3.1 The Time Discretization

First, the stiff source terms will be discretized implicitly in order to allow ε-independent time steps. Let $\Delta t > 0$ be the time step, and U^k denotes the numerical approximation of a general quantity

$U(t^k)$ where $t^k = k\Delta t$. The first step of the algorithm consists in updating the macroscopic unknowns $n, \rho, u, V, \Theta, \Upsilon$. We start with the uncoupled relations

$$\frac{1}{\Delta t}(n^{k+1} - n^k) = -\int_{\mathbb{R}^N} v \cdot \nabla_x f^k \, \mathrm{d}v = -\nabla_x \cdot (n^k V^k),$$
$$\frac{1}{\Delta t}(\rho^{k+1} - \rho^k) = -\nabla_x \cdot (\rho^k u^k),$$

which determines the densities n^{k+1} and ρ^{k+1}. Then, the velocities u^{k+1} and V^{k+1} are obtained by solving the system

$$\frac{1}{\Delta t}(n^{k+1}V^{k+1} - n^k V^k) = -\int_{\mathbb{R}^N} v \; v \cdot \nabla_x f^k \, \mathrm{d}v - \eta_P n^k \nabla_x \Phi + \frac{n^{k+1}}{\varepsilon}(V^{k+1} - u^{k+1}),$$
$$\frac{1}{\Delta t}(\rho^{k+1}u^{k+1} - \rho^k u^k) = -\mathrm{Div}_x(\rho^k u^k \otimes u^k + \rho^k \Theta^k) - \eta_F \rho^k \nabla_x \Phi - \frac{\rho_P}{\rho_F}\frac{n^{k+1}}{\varepsilon}(V^{k+1} - u^{k+1}).$$

Note that n^{k+1} has already been determined, and this step reduces to invert N 2×2 linear systems for each component of V^{k+1} and u^{k+1}, which can be inverted *analytically*. Finally, the temperature Θ and the energy Υ are updated with the system

$$\begin{aligned}
\frac{1}{\Delta t}(\Upsilon^{k+1} - \Upsilon^k) = &-\int \frac{v^2}{2} \; v \cdot \nabla_x f^k \, \mathrm{d}v - \eta_P n^k V^k \cdot \nabla_x \Phi \\
&-\frac{1}{\varepsilon}(2\Upsilon^{k+1} - n^{k+1}V^{k+1} \cdot u^{k+1} - N n^{k+1}\Theta^{k+1}), \\
\frac{1}{\Delta t}\Big(&\frac{\rho^{k+1}|u^{k+1}|^2 - \rho^k|u^k|^2}{2} + \frac{\rho^{k+1}\Theta^{k+1} - \rho^k\Theta^k}{\gamma - 1}\Big) \\
&= -\mathrm{div}_x\Big(\Big(\frac{\rho^k|u^k|^2}{2} + \frac{\gamma}{\gamma - 1}\rho^k\Theta^k\Big)u^k\Big) - \eta_F \rho^k u^k \cdot \nabla_x \Phi \\
&\quad + \frac{1}{\varepsilon}\frac{\rho_P}{\rho_F}(2\Upsilon^{k+1} - n^{k+1}V^{k+1} \cdot u^{k+1} - N n^{k+1}\Theta^{k+1}).
\end{aligned}$$

Since $n^{k+1}, u^{k+1}, V^{k+1}$ are already known, this step reduces to invert a 2×2 linear system for Υ^{k+1} and Θ^{k+1}, which can be done again *analytically*. Having at hand these quantities, one can update the Maxwellian $M^{k+1}(v) = M_{u^{k+1},\Theta^{k+1}}(v)$. The second step updates the particle distribution function by

$$\frac{1}{\Delta t}(f^{k+1} - f^k) = -(v \cdot \nabla_x f^k - \eta_P \nabla_x \Phi \cdot \nabla_v f^k) + \frac{\Theta^{k+1}}{\varepsilon}\mathrm{div}_v\Big(M^{k+1}\nabla_v\Big(\frac{f^{k+1}}{M^{k+1}}\Big)\Big).$$

Let us postpone for a while the question of inverting the Fokker–Planck operator, and start with some discussion on space and velocity discretizations.

3.2 Space and Velocity Discretizations

The convection terms can be treated as in [13], by coupling the upwind scheme in space and the center difference in velocity discretizations respectively for the kinetic equation with an anti-diffusive scheme of Finite Volume type [18, 33, 34] for the Euler system. However, we find it convenient to approximation the fluid equations by kinetic schemes which arise naturally from the fluid limit of the discretization of the kinetic equations, see [15, 16, 17, 42, 43, 44]. It is particularly well-suited to our model since the approximation of the microscopic and macroscopic equations will be based on the same discretization. Consequently, we will obtain naturally for $\varepsilon = 0$ a kinetic scheme for the system (9).

The idea consists in interpreting $\mathscr{U} = (\rho, \rho u, \rho E)$ as the zeroth, first and second order moments of a particle distribution function $G(t, x, v)$, subject to a strong relaxation. For the monoatomic

case, that is for $\gamma = (N+2)/N$ and thus $\rho E = \rho(|u|^2 + N\Theta)/2$, the Euler system

$$\partial_t \mathscr{U} + \nabla_x \begin{pmatrix} \rho u \\ \rho u^2 + \rho\Theta \\ \rho\big(|u|^2 + (N+2)\Theta\big)u/2 \end{pmatrix} = \bar{\mathbb{F}} - \eta_F \begin{pmatrix} 0 \\ \rho \\ \rho u \end{pmatrix} \partial_x \Phi \tag{10}$$

with a force field $\bar{\mathbb{F}} = \int_{\mathbb{R}^N} \mathbb{F}\,\mathrm{d}v$ can be derived from the limit for $\lambda \gg 1$ of the following BGK equation:

$$(\partial_t + v\nabla_x - \eta_F \partial_x \Phi \nabla_v) G = \mathbb{F} + \lambda(\mathscr{M}[G] - G)$$

with

$$\mathscr{M}[G] = \frac{\rho_G}{(2\pi\Theta_G)^{N/2}} \exp\Big(-\frac{|v-u_G|^2}{2\Theta_G}\Big),$$
$$\begin{pmatrix} \rho_G \\ \rho_G u_G \\ \rho_G |u_G|^2 + N\rho_G\Theta_G \end{pmatrix} = \int_{\mathbb{R}^N} \begin{pmatrix} 1 \\ v \\ v^2 \end{pmatrix} G\,\mathrm{d}v = \int_{\mathbb{R}^N} \begin{pmatrix} 1 \\ v \\ v^2 \end{pmatrix} \mathscr{M}[G]\,\mathrm{d}v.$$

We refer for instance to [9, 45] for results and comments on the analysis of this small mean free path regime. It leads to the following construction for solving (10), based on a time splitting of the BGK equation

- Define $G^\star$ from the transport equation

$$\frac{1}{\Delta t}(G^\star - G^k) + v \cdot \nabla_x G^k - \eta_F \nabla_x \Phi \cdot \nabla_v G^k = \mathbb{F}^{k+1}.$$

- Project the solution to the equilibrium state

$$G^{k+1} = \mathscr{M}[G^\star].$$

For describing a more general state law, one needs a coupled system of kinetic equations defined as follows:

$$(\partial_t + v \cdot \nabla_x - \eta_F \nabla_x \Phi \cdot \nabla_v) G_1 = \mathbb{F} + \lambda(\mathscr{M} - G_1),$$
$$\partial_t G_2 + v \cdot \nabla_x G_2 = \lambda(\mathscr{N} - G_2),$$

and still with $\lambda \gg 1$. A possible definition of $\mathscr{M}$ and $\mathscr{N}$ that generalizes the Maxwellian distribution is

$$\mathscr{M}(v) = \frac{\rho}{(2\pi\Theta)^{N/2}} \exp\Big(-\frac{|v-u|^2}{2\Theta}\Big),$$
$$\mathscr{N}(v) = \frac{2 - N(\gamma-1)}{2(\gamma-1)} \frac{\rho\Theta}{(2\pi\Theta)^{N/2}} \exp\Big(-\frac{|v-u|^2}{2\Theta}\Big),$$

where the macroscopic quantities are given by

$$\begin{pmatrix} \rho \\ \rho u \\ \dfrac{\rho|u|^2}{2} + \dfrac{\rho\Theta}{(\gamma-1)} \end{pmatrix} = \int_{\mathbb{R}^N} \begin{pmatrix} G_1 \\ vG_1 \\ \dfrac{v^2}{2}G_1 + G_2 \end{pmatrix} \mathrm{d}v = \int_{\mathbb{R}^N} \begin{pmatrix} \mathscr{M} \\ v\mathscr{M} \\ \dfrac{v^2}{2}\mathscr{M} + \mathscr{N} \end{pmatrix} \mathrm{d}v.$$

The scheme for the polytropic Euler system is now constructed as follows:

- Define $G_1^\star$ from the transport equation

$$\frac{1}{\Delta t}(G_1^\star - G_1^k) + v \cdot \nabla_x G_1^k - \eta_F \nabla_x \Phi \cdot \nabla_v G_1^k = \mathbb{F}^{k+1}$$

  and $G_2^\star$ from

$$\frac{1}{\Delta t}(G_2^\star - G_2^k) + v \cdot \nabla_x G_2^k = 0.$$

- Project the solution to the equilibrium state

$$G_1^{k+1} = \mathscr{M}, \qquad G_2^{k+1} = \mathscr{N},$$

with macroscopic quantities defined by moments of $G_1^\star$ and $G_2^\star$.

Of course this construction is fictitious since in the implementation of the kinetic schemes one only uses the macroscopic variables defined in physical space, which are obtained by taking moments on the above procedures, rather than the variable v or the microscopic quantities G_j. We refer to [15, 42], [43, Sections 1.7–1.10 & Section 8] or [25, Chapter III–Section 7] for a detailed introduction to kinetic schemes. The choice of equilibrium states based on the Maxwellian might look natural in view of the derivation of the Euler system from kinetic equations in the small mean free path regime, [9, 45]. In particular for the monoatomic case it leads to an elegant formula in the scheme for the coupled fluid/particles limit system, see (15) below. However, for numerical purposes other definitions of $\mathscr{M}$ and $\mathscr{N}$ are possible. In particular, dealing with compactly supported functions make stability issues clear [42, Theorem 3], [25, Proposition 7.3 & Theorem 7.2] and [43, Sections 1.7–1.10 & Section 8, sp. Theorem 8.3.1]. For instance, for the monoatomic case $\gamma = (N+2)/N$ ($\delta = 0$) one can use the follwoing compactly-supported function

$$\mathscr{M}[G] = \frac{1}{\mathrm{meas}(B_N)} \ \frac{\rho}{\big((N+2)\Theta)\big)^{N/2}} \ \mathbf{1}_{|v-u|\leq\sqrt{(N+2)\Theta}}$$

(remark that in dimension one, the monoatomic case corresponds to $\gamma = 3$). The numerical fluxes obtained this way coincides with Van Leer's fluxes, [25, Example 7.2].

Let us restrict the presentation of the space and velocity discretizations to the one-dimension framework. We consider a meshing of the domain, say $(-L, L)$, with J points separated by the step Δx. The velocity is truncated to the domain $(-V_{\mathrm{Max}}, +V_{\mathrm{Max}})$, discretized with a symmetric set of velocities $(v_1, ..., v_{2M})$, with step Δv. We denote by $f_{j,m}^k$ the numerical approximation of a microscopic quantity $f(k\Delta t, x_j, v_m)$ and set

$$\big\langle f \big\rangle_j^k = \frac{\Delta v}{2}\Big(f_{j,1}^k + f_{j,2M}^k + 2\sum_{m=2}^{2M-1} f_{j,m}^k \Big)$$

the approximation of the velocity average by the trapezoidal rule. This formula is chosen to ensure that the even moments of the odd functions with respect to v vanish, see [13]. For the sake of simplicity, we consider the simplest upwind discretization of the advection operator $v\partial_x$:

$v\partial_x(k\Delta t, x_j, v_m)$ is approximated by

$$vD_x[f]_{j,m}^k = \frac{1}{2\Delta x}\big((v_m + |v_m|)(f_{j,m}^k - f_{j-1,m}^k) + (v_m - |v_m|)(f_{j+1,m}^k - f_{j,m}^k)\big).$$

More elaborate version of the kinetic scheme can be used that reach second order accuracy and incorporate slope limiter to supress numerical oscillations across shocks, see [25, Section 7.3.4] and [42, Sections 2.2 & 4.2]. For the external force term, we can adopt a centered approximation of the $v-$derivative which yields, see [13]

$\partial_x\Phi\partial_v f(k\Delta t, x_j, v_m)$ is approximated by

$$vD_x[\Phi]_{j,m}^k \ \frac{1}{v_m} \ D_v[f]_{j,m}^k = vD_x[\Phi]_{j,m}^k \ \frac{1}{v_m} \ \frac{f_{j,m+1}^k - f_{j,m-1}^k}{2\Delta v}.$$

When the amplitude of the potential remains moderate compared to $1/\varepsilon$ it does not affect the stability of the scheme since the velocity diffusion term is treated implicitly in the Fokker–Planck operator. When the external force becomes large, upwinding has to be preferred; for instance

$\partial_x\Phi\partial_v f(k\Delta t, x_j, v_m)$ is approximated by

$$\frac{1}{2\Delta v}\Big((\partial_x\Phi_j - |\partial_x\Phi_j|)(f_{j,m}^k - f_{j,m-1}^k) + (\partial_x\Phi_j + |\partial_x\Phi_j|)(f_{j,m+1}^k - f_{j,m}^k)\Big).$$

Remark 3.1 *In numerical simulation we are applying the following second order finite volume scheme on the external force term. (In fact the x derivative term is solved by the same scheme.)*

$\partial_x\Phi\partial_v f(k\Delta t, x_j, v_m)$ is approximated by
$$\frac{1}{2\Delta v}\Big((\partial_x\Phi_j - |\partial_x\Phi_j|)(F^+_{j,m+1/2} - F^+_{j,m-1/2}) + (\partial_x\Phi_j + |\partial_x\Phi_j|)(F^-_{j,m+1/2} - F^-_{j,m-1/2})\Big),$$

with

$$F^+_{j,m+1/2} = f_{j,m} + \sigma_{j,m}\frac{f_{j,m+1} - f_{j,m}}{2}$$

$$F^-_{j,m+1/2} = f_{j,m+1} - \sigma_{j,m+1}\frac{f_{j,m+1} - f_{j,m}}{2}$$

and

$$\sigma_{j,m} = \phi\left(\frac{f_{j,m} - f_{j,m-1}}{f_{j,m+1} - f_{j,m}}\right)$$

where the limiter function $\phi(\theta)$ is, for example, the van Leer limiter

$$\phi(\theta) = \frac{\theta + |\theta|}{1 + |\theta|}$$

or the minmod limiter

$$\phi(\theta) = \max\{0, \min\{1, \theta\}\}.$$

This discretization is stable as long as $\frac{|\partial_x\Phi|\Delta t}{\Delta v} \le \frac{1}{2}$.

Finally, given discrete density, velocity and temperature $(\rho^k_j, u^k_j, \Theta^k_j)$, denote

$$M^k_{j,m} = \frac{1}{\sqrt{2\pi\Theta^k_j}}\exp\Big(-\frac{|v_m - u^k_j|^2}{2\Theta^k_j}\Big),$$
$$\mathscr{M}^k_{j,m} = \frac{\rho^k_j}{\sqrt{2\pi\Theta^k_j}}\exp\Big(-\frac{|v_m - u^k_j|^2}{2\Theta^k_j}\Big), \qquad \mathscr{N}^k_{j,m} = \frac{2-(\gamma-1)}{2(\gamma-1)}\frac{\rho^k_j\Theta^k_j}{\sqrt{2\pi\Theta^k_j}}\exp\Big(-\frac{|v_m - u^k_j|^2}{2\Theta^k_j}\Big),$$

and $\mathscr{L}f^k_{j,m}$ the corresponding approximation of $L_{u,\Theta}f$ at $(k\Delta t, x_j, v_m)$. The precise form of this approximation will be detailed in the next section. Then the fully discretized form of the algorithm reads as follows

- Step 1. Updating the macroscopic quantities: Find $(\rho^{k+1}_j, n^{k+1}_j, u^{k+1}, V^{k+1}_j, \Theta^{k+1}_j, \Upsilon^{k+1}_j)$

which are solution of

$$
\begin{aligned}
&\frac{1}{\Delta t}(n_j^{k+1}-n_j^k) = -\big\langle vD_x[f]\big\rangle_j^k,\\
&\frac{1}{\Delta t}(\rho_j^{k+1}-\rho_j^k) = -\big\langle vD_x[\mathscr{M}]\big\rangle_j^k,\\
&\frac{1}{\Delta t}(n_j^{k+1}V_j^{k+1}-n_j^kV_j^k) = -\big\langle v\ vD_x[f]\big\rangle_j^k + \eta_P\Big\langle vD_x[\Phi]\ D_v[f]\Big\rangle_j^k + \frac{n_j^{k+1}}{\varepsilon}(V_j^{k+1}-u_j^{k+1}),\\
&\frac{1}{\Delta t}(\rho_j^{k+1}u_j^{k+1}-\rho_j^ku_j^k) = -\big\langle v\ vD_x[\mathscr{M}]\big\rangle_j^k + \eta_F\Big\langle vD_x[\Phi]\ D_v[\mathscr{M}]\Big\rangle_j^k - \frac{\rho_P}{\rho_F}\frac{n_j^{k+1}}{\varepsilon}(V_j^{k+1}-u_j^{k+1}),\\
&\frac{1}{\Delta t}(\Upsilon_j^{k+1}-\Upsilon_j^k) = -\Big\langle\frac{v^2}{2}vD_x[f]\Big\rangle_j^k + \eta_P\Big\langle vD_x[\Phi]\ \frac{v}{2}D_v[f]\Big\rangle_j^k\\
&\qquad\qquad -\frac{1}{\varepsilon}(2\Upsilon_j^{k+1}-n_j^{k+1}V_j^{k+1}\cdot u_j^{k+1}-n_j^{k+1}\Theta_j^{k+1}),\\
&\frac{1}{\Delta t}\Big(\frac{\rho_j^{k+1}|u_j^{k+1}|^2-\rho_j^k|u_j^k|^2}{2}+\frac{\rho_j^{k+1}\Theta_j^{k+1}-\rho_j^k\Theta_j^k}{\gamma-1}\Big)\\
&\quad = -\Big\langle\frac{v^2}{2}vD_x[\mathscr{M}]\Big\rangle_j^k - \big\langle vD_x[\mathscr{N}]\big\rangle_j^k + \eta_F\Big\langle vD_x[\Phi]\ \frac{v}{2}D_v[\mathscr{M}]\Big\rangle_j^k\\
&\qquad\qquad +\frac{1}{\varepsilon}\frac{\rho_P}{\rho_F}(2\Upsilon_j^{k+1}-n_j^{k+1}V_j^{k+1}\cdot u_j^{k+1}-n_j^{k+1}\Theta_j^{k+1}).
\end{aligned}
\tag{11}
$$

- Step 2. Updating the particle distribution function. The first step allows to define $M_{j,m}^{k+1}$. Then, we define $f_{j,m}^{n+1}$ as the solution of

$$
\frac{1}{\Delta t}(f_{j,m}^{k+1}-f_{j,m}^k) = -vD_x[f]_{j,m}^k + \eta_P vD_x[\Phi]_{j,m}^k\frac{1}{v}D_v[f]_{j,m}^k + \frac{1}{\varepsilon}\mathscr{L}f_{j,m}^{k+1}. \tag{12}
$$

  It requires the inversion of the operator $(1-\frac{\Delta t}{\varepsilon}\mathscr{L})$ that will be discussed in the next subsection. We finish the time step by setting

$$
n_j^{k+1} = \big\langle f\big\rangle_j^{k+1}, \qquad n_j^{k+1}V_j^{k+1} = \big\langle vf\big\rangle_j^{k+1}, \qquad \Upsilon_j^{k+1} = \frac{1}{2}\big\langle v^2f\big\rangle_j^{k+1}.
$$

Remark 3.2 *For the boundary condition, we apply the specular reflection law for the particles. For the discrete unknown, it casts as*

$$
f_{0,2M+1-m}^k = f_{1,m}^k, \qquad f_{J+1,m}^k = f_{J,2M+1-m}^k.
$$

For the hydrodynamic unknowns, we use the so-called "wall boundary condition" which are imposed through ghost cells

$$
\big(\rho_0^k,u_0^k,\Theta_0^k\big) = \big(\rho_1^k,-u_1^k,\Theta_1^k\big), \quad \big(\rho_{J+1}^k,u_{J+1}^k,\Theta_{J+1}^k\big) = \big(\rho_J^k,-u_J^k,\Theta_J^k\big).
$$

We refer for instance to [1] for discussion of numerical boundary conditions for kinetic schemes.

Remark 3.3 *In many situation $\partial_x\Phi = \Psi$ has a simple expression. For instance it is merely constant for gravity–driven flows. Then, the external force terms in* (11) *is replaced by $\eta_P n_j^k\Psi_j$, $\eta_P n_j^kV_j^k\Psi_j$, $\eta_F\rho_j^k\Psi_j$, $\eta_F\rho_j^ku_j^k\Psi_j$.*

3.3 Treatment of the Fokker-Planck operator

We follow the method introduced in [32]. Given u and Θ, it is convenient to write

$$
L_{u,\Theta}f = \Theta\sqrt{M_{u,\Theta}}\ \tilde{L}_{u,\Theta}h
$$

with

$$h = \frac{f}{\sqrt{M_{u,\Theta}}}, \qquad \tilde{L}_{u,\Theta} h = \frac{1}{\sqrt{M_{u,\Theta}}} \mathrm{div}_v \Big(M_{u,\Theta} \nabla_v \Big(\frac{h}{\sqrt{M}_{u,\Theta}} \Big) \Big).$$

The advantage of this change of unknown lies on the symmetry property

$$\int_{\mathbb{R}^N} \tilde{L}_{u,\Theta} h \; g \, \mathrm{d}v = \int_{\mathbb{R}^N} h \; \tilde{L}_{u,\Theta} g \, \mathrm{d}v.$$

Accordingly, we set

$$h_{j,m} = \frac{f_{j,m}^{k+1}}{\sqrt{M_{j,m}^{k+1}}}, \qquad \mathscr{L} f_{j,m}^{k+1} = \Theta_j^{k+1} \sqrt{M_{j,m}^{k+1}} \; \tilde{\mathscr{L}} h_{j,m},$$

where the discrete operator $\tilde{\mathscr{L}}$ will be symmetric which allows the inversion of the implicit term by the effective the Conjugate Gradient algorithm. Therefore, Step 2 of the alorithm can be recast as follows:

- Solve the linear system

$$\big(1 - \frac{\Delta t}{\varepsilon} \Theta_j^{k+1} \tilde{\mathscr{L}}\big) h_{j,m} = \frac{f_{j,m}^k}{\sqrt{M_{j,m}^{k+1}}} - \frac{\Delta t}{\sqrt{M_{j,m}^{k+1}}} \Big(v D_x [f]_{j,m}^k - \eta_P v D_x [\Phi]_{j,m}^k \frac{1}{v} D_v [f]^k \Big).$$

- Set $f_{j,m}^{k+1} = h_{j,m} \sqrt{M_{j,m}^{k+1}}$.

In the one–dimension setting, the discrete operator $\tilde{\mathscr{L}}$ is defined as follows, see [32]

$$\tilde{\mathscr{L}} h_{j,m} = \frac{1}{\Delta v^2} \left(h_{j,m+1} - \frac{\sqrt{M_{j,m+1}^{k+1}} + \sqrt{M_{j,m-1}^{k+1}}}{\sqrt{M_{j,m}^{k+1}}} h_{j,m} + h_{j,m-1} \right) \tag{13}$$

which indeed leads to a symmetric matrix. Observe that $\tilde{\mathscr{L}} \big(\sqrt{M^{k+1}} \big)_{j,m} = 0$.

Lemma 3.4 *Consider the discrete operator* (13) *with the Neumann-like conditions*

$$\begin{array}{l} \sqrt{M_{j,1}} (h_{j,0} - h_{j,2}) + h_{j,1} (\sqrt{M_{j,2}} - \sqrt{M_{j,0}}) = 0, \\ \sqrt{M_{j,2M}} (h_{j,2M-1} - h_{j,2M+1}) + h_{j,2M} (\sqrt{M_{j,2M+1}} - \sqrt{M_{j,2M-1}}) = 0. \end{array} \tag{14}$$

Then, the operator is mass–conserving in the sense that

$$\big\langle \sqrt{M} \tilde{\mathscr{L}} h \big\rangle = 0,$$

and entropy–decaying in the sense that

$$\big\langle \sqrt{M} \tilde{\mathscr{L}} h \ln \big(h / \sqrt{M} \big) \big\rangle \leq 0.$$

Remark 3.5 *Note that the definition of the ghost points with respect to the velocity variable depends on the discrete integration rule: if the rectangle rule is used then one should replaces*(14) *by* $\frac{h_{j,0}}{\sqrt{M_{j,0}}} = \frac{h_{j,1}}{\sqrt{M_{j,1}}}$ *and* $\frac{h_{j,2M+1}}{\sqrt{M_{j,2M+1}}} = \frac{h_{j,2M}}{\sqrt{M_{j,2M}}}$. *The definition looks like an approximation of the Neumann–like boundary condition* $M \partial_v (\frac{h}{\sqrt{M}}) = 0 = M \partial_v (f/M)$.

Proof. The key argument relies on the observation

$$\begin{array}{rcl} \sqrt{M_m} \left(h_{m+1} - \dfrac{\sqrt{M_{m+1}} + \sqrt{M_{m-1}}}{\sqrt{M_m}} h_m + h_{m-1} \right) & = & \sqrt{M_{m+1} M_m} \left(\dfrac{h_{m+1}}{\sqrt{M_{m+1}}} - \dfrac{h_m}{\sqrt{M_m}} \right) \\ & & - \sqrt{M_m M_{m-1}} \left(\dfrac{h_m}{\sqrt{M_m}} - \dfrac{h_{m-1}}{\sqrt{M_{m-1}}} \right). \end{array}$$

It allows to conclude by summation by parts. □

3.4 Properties of the scheme

Asymptotic Preserving
We can study the limit of the scheme as ε goes to 0. First, Step 2 enforces $f_{j,m}^{k+1}$ to coincide with the discrete Maxwellian $n_j^{k+1}M_{j,m}^{k+1}$. Then, adding the two momentum equations and the two energy equations and replacing f by the Maxwellian in (11), we obtain

$$
\begin{aligned}
&\frac{1}{\Delta t}(n_j^{k+1}-n_j^k) = -\big\langle vD_x[nM]\big\rangle_j^k,\\
&\frac{1}{\Delta t}(\rho_j^{k+1}-\rho_j^k) = -\big\langle vD_x[\mathscr{M}]\big\rangle_j^k,\\
&\frac{1}{\Delta t}\Big(\Big(\rho_j^{k+1}+\frac{\rho_P}{\rho_F}n_j^{k+1}\Big)u_j^{k+1}-\Big(\rho_j^k+\frac{\rho_P}{\rho_F}n_j^k\Big)u_j^k\Big)\\
&\qquad = -\Big\langle v\ vD_x\Big[\mathscr{M}+\frac{\rho_P}{\rho_F}nM\Big]\Big\rangle_j^k + \eta_P\Big\langle vD_x[\Phi]\ \frac{1}{v}D_v\Big[(\eta_F\mathscr{M}+\eta_P\frac{\rho_P}{\rho_F}nM\Big]\Big\rangle_j^k\\
&\frac{1}{2\Delta t}\Big(\frac{\Big(\rho_j^{k+1}+\frac{\rho_P}{\rho_F}n_j^{k+1}\Big)|u_j^{k+1}|^2-\Big(\rho_j^k+\frac{\rho_P}{\rho_F}n_j^k\Big)|u_j^k|^2}{2}+\frac{\rho_j^{k+1}\Theta_j^{k+1}-\rho_j^k\Theta_j^k}{\gamma-1}+\frac{\rho_P}{\rho_F}\frac{n_j^{k+1}\Theta_j^{k+1}-n_j^k\Theta_j^k}{2}\Big)\\
&\qquad = -\Big\langle\frac{v^2}{2}vD_x\Big[(\mathscr{M}+\frac{\rho_P}{\rho_F}nM\Big]\Big\rangle_j^k + \big\langle vD_x[\mathscr{N}]\big\rangle_j^k + \Big\langle vD_x[\Phi]\ \frac{v}{2}D_v\Big[(\eta_F\mathscr{M}+\eta_F\frac{\rho_P}{\rho_F}nM\Big]\Big\rangle_j^k.
\end{aligned}
\tag{15}
$$

This is exactly a kinetic scheme for the limit system (9). Note that this expression simplifies in the monoatomic case when we use the Maxwellian $\rho_j^k M_{j.m}^k$ as distribution $\mathscr{M}_{j,m}^k$.

Well-Balance
It turns out that stationary solutions are defined by

$$
\begin{aligned}
&f_S(x,v) = Z_P\exp\Big(-\frac{v^2}{2\Theta}-\frac{\eta_P\Phi(x)}{\Theta}\Big),\\
&\rho_S(x) = Z_F\exp\Big(-\frac{\eta_F\Phi(x)}{\Theta}\Big), \qquad u(x)=0, \qquad \Theta>0 \text{ (constant)},
\end{aligned}
$$

with Z_F and Z_P normalizing constants. For instance one can set

$$
Z_P = \frac{M_P}{\rho_P(2\pi\Theta)^{N/2}}\Big(\int e^{-\eta_P\Phi(x)/\Theta}\,\mathrm{d}x\Big)^{-1}, \qquad Z_F = \frac{M_F}{\rho_F}\Big(\int e^{-\eta_F\Phi(x)/\Theta}\,\mathrm{d}x\Big)^{-1}
$$

where M_P and M_F correspond to the masses of the disperse and the dense phases respectively. The stationary solutions can be expected to be natural candidates for describing the large time behavior of the solutions, with the parameters M_F, M_P and Θ determined by the conservation relations

$$
M_P = \rho_P\int f(0,x,v)\,\mathrm{d}v\,\mathrm{d}x, \qquad M_F = \rho_F\int\rho(0,x)\,\mathrm{d}x,
$$

together with

$$
\rho_P\int\Big(\frac{v^2}{2}+\eta_P\Phi(x)\Big)f_S(x,v)\,\mathrm{d}v\,\mathrm{d}x + \rho_F\int\Big(\frac{\Theta}{\gamma-1}+\eta_F\Phi(x)\Big)\rho_S(x)\,\mathrm{d}x = E_0
$$

where E_0 stands for the total energy given by

$$
E_0 = \rho_P\int\Big(\frac{v^2}{2}+\eta_P\Phi(x)\Big)f(0,x,v)\,\mathrm{d}\,\mathrm{d}x + \rho_F\int\Big(\frac{|u(0,x)|^2}{2}+\frac{\Theta(0,x)}{\gamma-1}+\eta_F\Phi(x)\Big)\rho(0,x)\,\mathrm{d}x.
$$

It can be recast as

$$
M_P\big(N\Theta+\mathscr{P}_P(\Theta)\big)+M_F\Big(\frac{\Theta}{\gamma-1}+\mathscr{P}_F(\Theta)\Big) = E_0 \tag{16}
$$

where $\mathscr{P}_P$ and $\mathscr{P}_F$ depend on the potential Φ:

$$\mathscr{P}_P = \frac{\displaystyle\int \eta_P \Phi(x) e^{-\eta_P \Phi(x)/\Theta}\,\mathrm{d}x}{\displaystyle\int e^{-\eta_P \Phi(x)/\Theta}\,\mathrm{d}x}, \qquad \mathscr{P}_F = \frac{\displaystyle\int \eta_F \Phi(x) e^{-\eta_F \Phi(x)/\Theta}\,\mathrm{d}x}{\displaystyle\int e^{-\eta_F \Phi(x)/\Theta}\,\mathrm{d}x}.$$

Observe that

$$\begin{aligned}\frac{\mathrm{d}}{\mathrm{d}\Theta}\mathscr{P}(\Theta) &= \frac{1}{\left(\Theta \displaystyle\int e^{-\eta_P \Phi(x)/\Theta}\,\mathrm{d}x\right)^2} \\ &\quad \times \left(\int \left|\eta_P \Phi(x)\right|^2 e^{-\eta_P \Phi(x)/\Theta}\,\mathrm{d}x \int e^{-\eta_P \Phi(x)/\Theta}\,\mathrm{d}x - \left(\int \eta_P \Phi(x) e^{-\eta_P \Phi(x)/\Theta}\,\mathrm{d}x\right)^2\right)\end{aligned}$$

is non–negative as a consequence of the Cauchy-Schwarz inequality. Therefore (16) uniquely defines $\Theta \geq 0$ for any $E_0 \geq 0$. Modulus $\mathscr{O}(\Delta x)$ and $\mathscr{O}(\Delta v)$ errors the stationary solutions are preserved by the scheme. If the center difference is used for the external force term, the velocity error becomes of order $\mathscr{O}(\Delta v^2)$ and furthermore it only involves odd terms with respect to v, so that its velocity average vanishes [13].

4 Numerical simulations

We perform numerical simulation in the one dimension framework, bearing in mind the example of gravity driven flows. The spacial domain is the slab $[0, 1]$, where x is thought of as a "vertical" variable (with $x = 0$ corresponding to the bottom and $x = 1$ to the top). The velocity variable lies in the truncated domain $v \in [-V_{\mathrm{Max}}, V_{\mathrm{Max}}]$, and for the simulation we set $V_{\mathrm{Max}} = 6$. In our numerical experiments, the units are chosen such that the gravity constant is $g = 1$ for the sake of simplicity. The initial particle distribution function has the form

$$f(0, x, v) = \frac{n(0, x)}{\sqrt{2\pi\Theta_P(0, x)}} \exp\left(-\frac{|v - V(0, x)|^2}{2\Theta_P(0, x)}\right). \tag{17}$$

Notice that this distribution is not at equilibrium as far as $V(0, x) \neq u(0, x)$, or $\Theta_P(0, x) \neq \Theta(0, x)$ with $u(0, x)$ and $\Theta(0, x)$ the initial velocity and temperature fields of the fluid, respectively. Finally, the numerical parameters are $\Delta t = 0.4\frac{\Delta x}{V_{\mathrm{Max}}}$. This choice guarantees the stability of the simulation.

4.1 Energy conservation and entropy dissipation

To start with, we check the ability of the scheme in preserving mass, energy and in dissipating entropy, according to (6) and (7). For the simulation we present, we consider initially an homogeneous fluid at rest:

$$\rho(0, x) = 1, \qquad u(0, x) = 0, \qquad \Theta(0, x) = 1. \tag{18}$$

The distribution of particles is given by (17) with

$$n(0, x) = 0.5 + \exp(-160(x - 0.5)^2), \qquad V(0, x) = 0, \qquad \Theta_P(0, x) = 1. \tag{19}$$

We set $\varepsilon = 0.1$, and $\rho_P/\rho_F = 5$ while the adiabatic constant is $\gamma = 1.4$. The results to be discussed do not significantly change when these parameters vary. Although will not be shown by a figure here, owing to the treatment of the boundary condition, the total mass of both phases is exactly conserved numerically. Figure 1(a) shows the time evolution up to the final time $T = 20$ of the total energy, which is a discrete version of (6). The discrete energy is not exactly conserved, but by varying the mesh size one can observe that the error remains of order $\mathscr{O}(\Delta x)$. This discrepancy

can be explained by the influence of the boundary terms that remain when performing the discrete integration by parts in the energy balance.

Next we study the evolution of the entropy. The discretized entropy at time t^n is defined by

$$H^n = \rho_F \int_{\mathbb{R}} \rho^n S^n \,\mathrm{d}x + \rho_P \int_{\mathbb{R}} \int_{\mathbb{R}} f^n \ln(f^n) \,\mathrm{d}v \,\mathrm{d}x$$

where the numerical integration is done by the trapezoidal rule for v and the rectangle rule for x. In Figure 1(b) we compare the discrete time derivative $\frac{H^{n+1}-H^n}{\Delta t}$ (blue line) and the dissipation term which is a discrete analog of the right hand side of (7) (dotted red line). More exactly, the discretized dissipation term is computed based on the equivalent form

$$\frac{\mathrm{d}}{\mathrm{d}t} H = -\frac{\rho_P}{\varepsilon} \left(\int_{\mathbb{R}^N} \int_{\mathbb{R}^N} \frac{\Theta}{f} \Big| M_{V,\Theta} \nabla_v \frac{f}{M_{V,\Theta}} \Big|^2 \,\mathrm{d}v \,\mathrm{d}x + \int_{\mathbb{R}^N} \int_{\mathbb{R}^N} f \frac{|V-u|^2}{\Theta} \,\mathrm{d}v \,\mathrm{d}x \right). \tag{20}$$

They are not identical but their evolutions have the same qualitative features. In particular it is remarkable that $\frac{H^{n+1}-H^n}{\Delta t}$ remains negative, establishing a numerical evidence of the decay of entropy.

Finally we consider the evolution of the (macroscopic) kinetic energy of the two phases

$$K_f = \rho_F \int_{\mathbb{R}} \rho u^2 \,\mathrm{d}x, \qquad K_p = \rho_P \int_{\mathbb{R}} n V^2 \,\mathrm{d}x.$$

The numerical simulation shows that both quantities are decaying, with oscillations presenting a very similar shape, which suggests that the solutions are approaching some stationary state. This is confirmed by Figure 2 where we compare the solution at time $T = 20$ with the stationary solution having the same mass and energy. We take $\rho_P/\rho_F = 5$ and $\rho_P/\rho_F = 0.5$, which give different monotonicities in the density profile of particles in stationary solution. The agreement is quite good, with discrepancies that can be explained either by a final time not large enough or by the defect in the energy conservation.

4.2 Effects of the density ratio ρ_P/ρ_F

Now we study the influence of the external force. We remind that for the case of gravity–driven flows, we have $\eta_F = 1$ and $\eta_P = 1 - \rho_F/\rho_P$. Therefore the sign of η_P determines whether the movement of particles is gravity dominated (corresponding to the "+" sign), or buoyancy dominated (corresponding to the "−" sign).

At first, we investigate the standard model where ρ_P and ρ_F are constants, corresponding to the mass density of the particles and a typical mass density of the fluid, respectively. We vary the ratio ρ_P/ρ_F. The simulation is performed with the uniform initial data (18) for the fluid, while the particles are initially at rest, concentrated at the center of the domain

$$n(0,x) = \mathbf{1}_{[0.3,0.7]}(x), \qquad V(0,x) = 0, \qquad \Theta_P(0,x) = 1.$$

The numerical profiles of the hydrodynamic unknowns at final time $T = 0.4$ are shown in Figure 3, with different values of ρ_P/ρ_F. We take $\varepsilon = 1$, $\gamma = 1.4$, on the grid $N_x = 50$, $N_v = 32$.

Since the fluid is only subject to gravity, the fluid always moves downwards and its density near the bottom ($x = 0$) is always higher. By contrast, the particle's repartition depends on the relative value of ρ_P/ρ_F compared to 1. The movement of particles is dominated by buoyancy when $\rho_P/\rho_F < 1$: Figure 3(a) shows that particles concentrate near the top. When ρ_P/ρ_F tends to 1, the gravity balances the buoyancy and the particles moves freely. But due to the interaction with the fluid, the downward direction is more favored in the movement of particles, as shown in Figure 3(b).

When we consider heavy particles, i.e. $\rho_P/\rho_F > 1$, both phases are dominated by gravity, as in Figure 3(c)(d) and the two densities are higher at the bottom as time becomes large. It is also

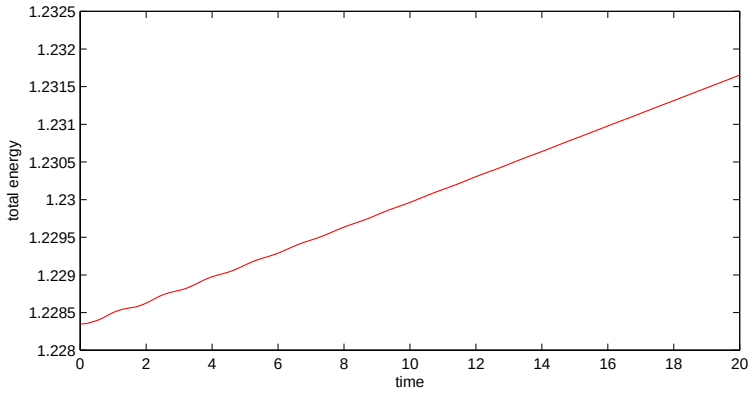

(a) energy conservation

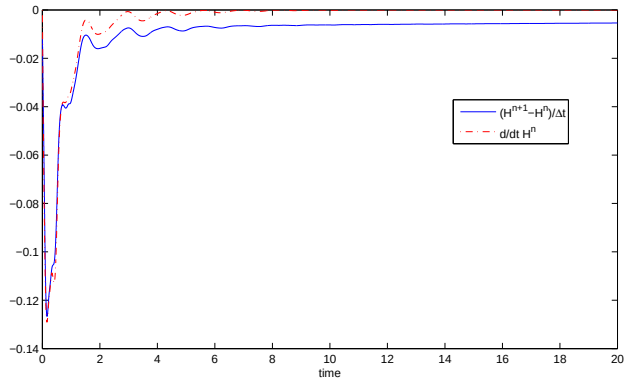

(b) entropy dissipation

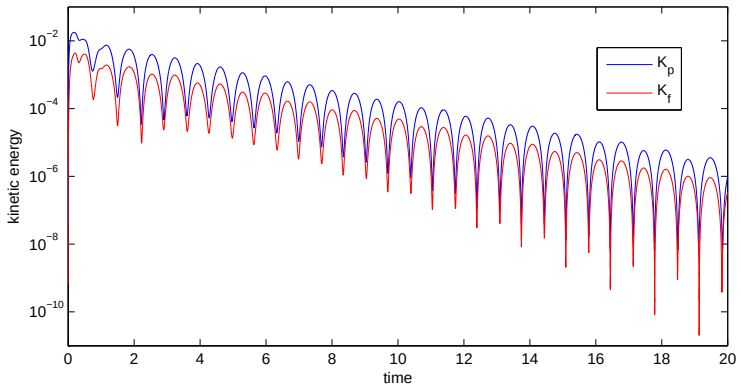

(c) decay of kinetic entropy

Figure 1: Time evolution of the total energy, total entropy and the kinetic energy of the two phases. Here $\gamma = 1.4$, $\varepsilon = 0.1$, $\rho_P/\rho_F = 5$, $N_x = 1000$, $N_v = 32$.

worth remarking that particles act like a wall for the fluid, resulting in a clear separation of the domain; this is particularly sensible at the beginning of the simulation when a large amount of particles is located at the center of the domain. We also point out that the scheme is able to handle

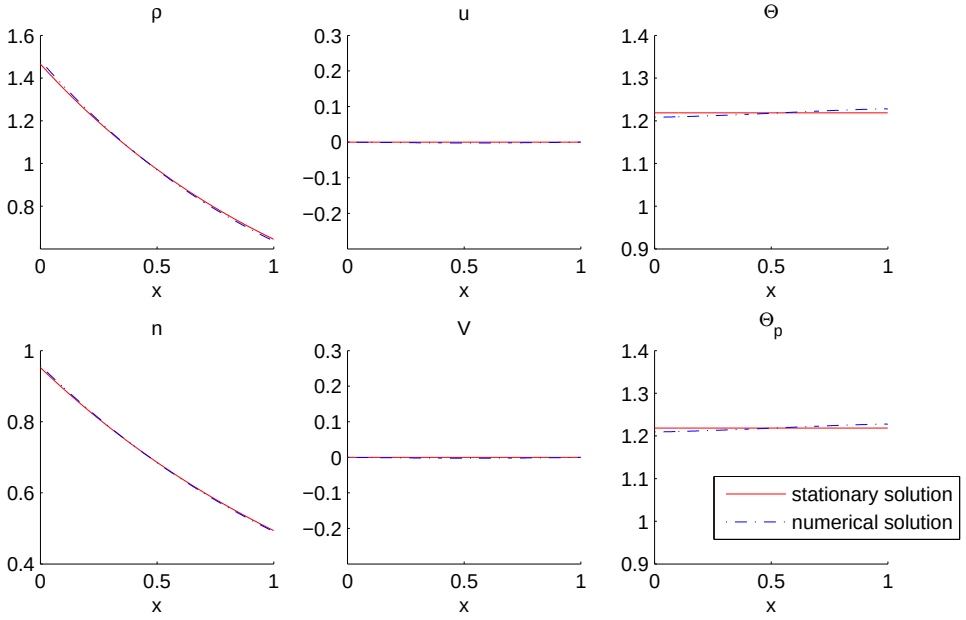

(a) $\rho_P/\rho_F = 5$.

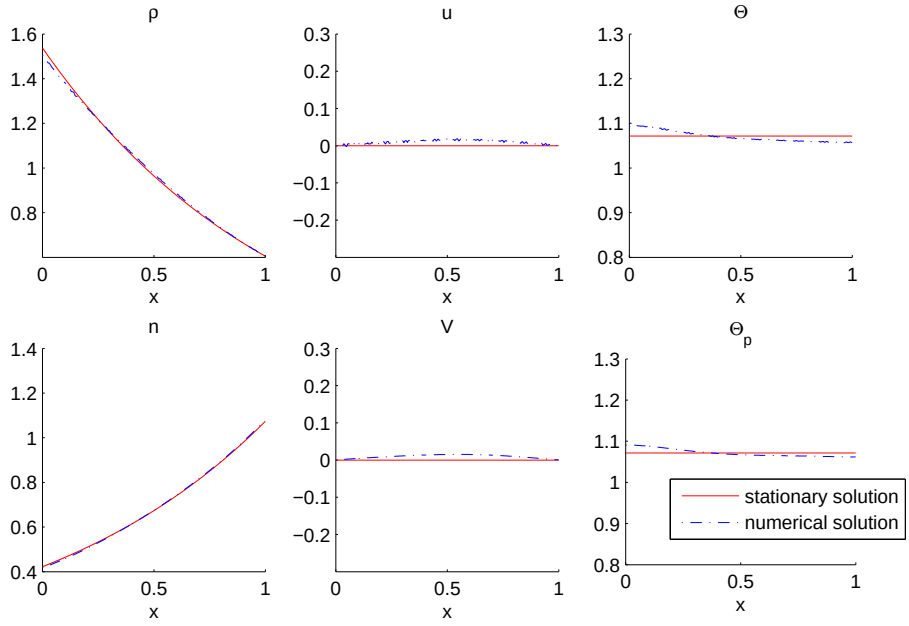

(b) $\rho_P/\rho_F = 0.5$.

Figure 2: Comparison of the solution (blue dashed lines) at final time $T = 20$ to the stationary solution (red solid lines) having the same mass and energy, with different ρ_P/ρ_F. Here $\gamma = 1.4$, $\varepsilon = 0.1$, $N_x = 1000$, $N_v = 32$.

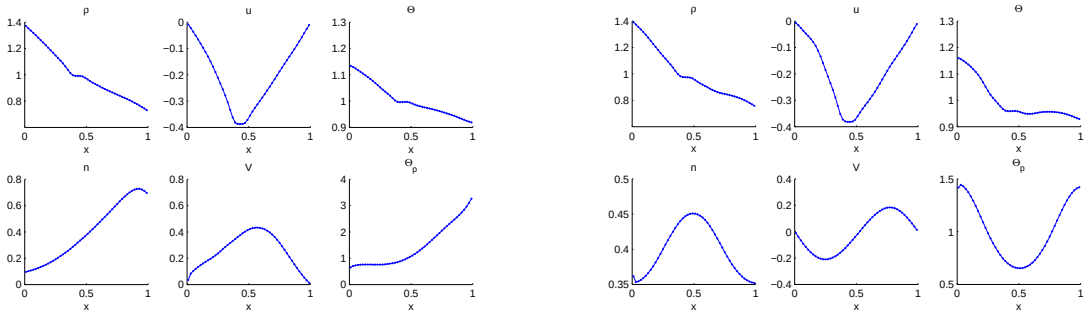

(a) $\frac{\rho_P}{\rho_F} = 0.2$ (b) $\frac{\rho_P}{\rho_F} = 0.9$

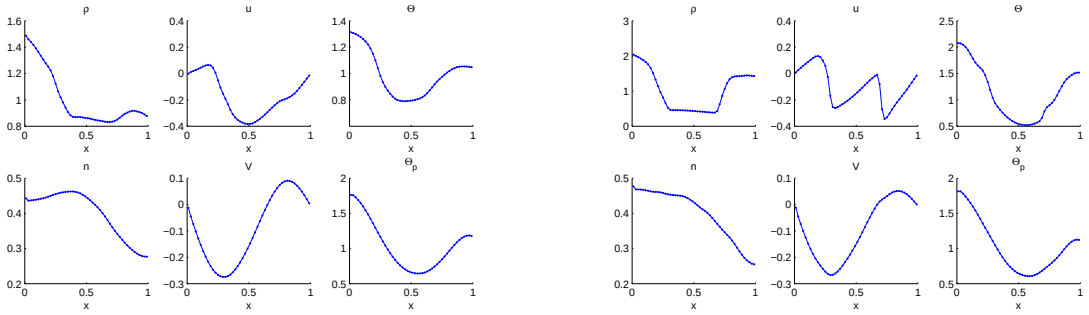

(c) $\frac{\rho_P}{\rho_F} = 5$ (d) $\frac{\rho_P}{\rho_F} = 100$

Figure 3: Macroscopic profiles for the fluid (up) and the particles (down) at $T = 0.4$, with different ρ_P/ρ_F. Here $\gamma = 1.4$, $\varepsilon = 1$.

cases with high density ratio, with particles much heavier than the fluid.

It might be questionable to consider a constant reference fluid density in the expression of the buoyancy force because the model makes the fluid density vary and might create zones of low (resp. high.) density. Therefore we perform a couple of simulations by changing ρ_F to $\rho_F \times \rho(t,x)$ in the definition of the buoyancy force. Note however that such a model induces severe technical issues; in particular in this case the force acting on the particles cannot be derived from a potential and the energy balance becomes unclear. Nevertheless the simulation brings out some interesting phenomena. We set the initial density of the fluid to be a piecewise constant, so that the motion of particles are gravity driven in some domains and buoyancy driven in the others:

$$\begin{array}{lll} \rho(0,x) = \frac{1}{4} + \frac{3}{2}\mathbf{1}_{x<1/2}, & u(0,x) = 0, & \Theta(0,x) = 1\,, \\ n(0,x) = 1, & V(0,x) = 0, & \Theta_P(0,x) = 1\,. \end{array}$$

We take $\varepsilon = 1$, $\gamma = 1.4$ on the grid $N_x = 50$, $N_v = 32$. The profiles of the macroscopic quantities at $T = 0.2$ are shown in Figure 4, which compares the standard model with a constant reference fluid density (see Figure 4(a)) and the case that takes density variation into account (see Figure 4(b)). The motion of the fluid does not change too much, but the particles move differently, with a clear tendency towards the interface $x = \frac{1}{2}$.

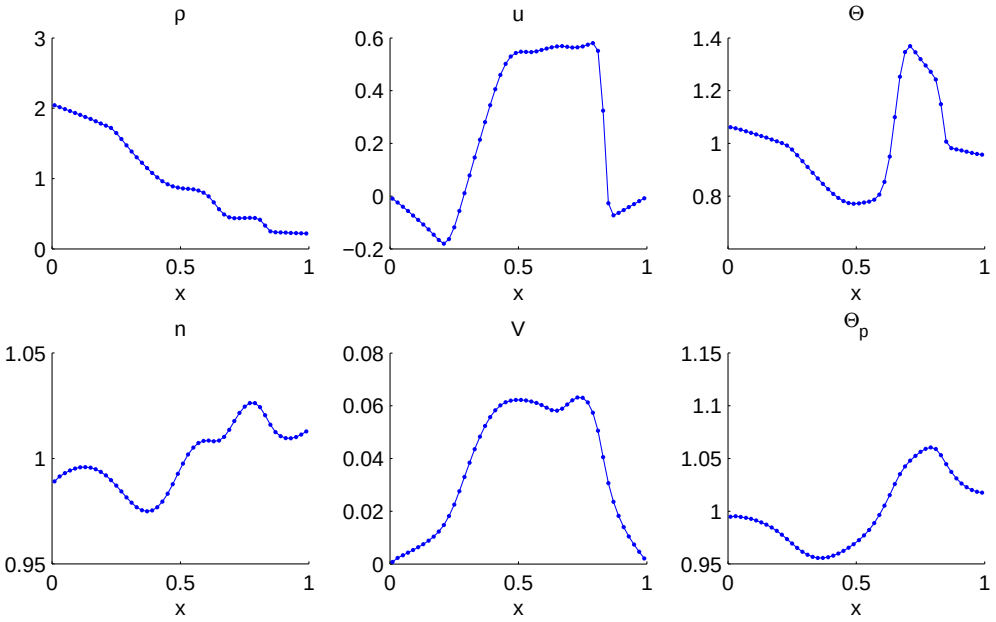

(a) constant ρ_F, with $\rho_P/\rho_F = 0.9$.

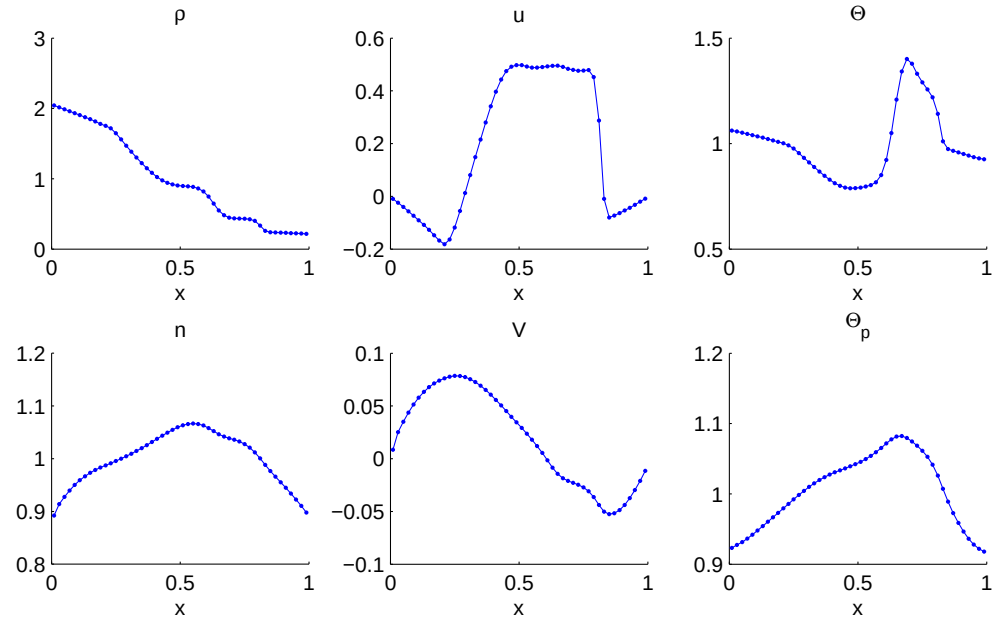

(b) x-dependent ρ_F, given by the density of fluid

Figure 4: Macroscopic profiles for the fluid (up) and the particles (down) at $T = 0.2$: comparison of the model with constant and variable coefficients in the buoyancy force. Here $\gamma = 1.4$, $\varepsilon = 1$.

4.3 Asymptotic Preserving properties: vanishing Stokes number

In this section we investigate the behavior of the numerical solution as the parameter ε goes to 0. We take $\gamma = 1.4$, $\frac{\rho_P}{\rho_F} = 2$. The initial data is defined as in (18) and (17) with

$$n(0,x) = 0.5 + \exp(-160(x-0.5)^2), \qquad V(0,x) = \exp(-160(x-0.5)^2), \qquad \Theta_P(0,x) = 1.$$

We perform simulations with different Stokes number ε, on the same grid $N_x = 50$, $N_v = 32$. The results at $T = 0.3$ are displayed in Figure 5. As ε gets smaller, the effects of friction between the two different phases become more and more prominent. The buoyancy effect is dominated by the friction in the case $\varepsilon = 10^{-4}$. We observe the (fast) equilibration of the velocities $u = V$, and temperatures $\Theta = \Theta_P$, as expected from the entropy dissipation and the formal derivation. In order to evaluate in a quantitative way this effect, we introduce the ℓ^1 distance between the particle distribution f and the equilibrium $nM_{u,\Theta}$,

$$\mathrm{dist}(t) = \|f(t,x,v) - nM_{u,\Theta}(t,x,v)\|_1. \tag{21}$$

The time evolution of dist(t) for different values of ε is shown in Figure 6. As $\varepsilon \to 0$, it shows a numerical evidence that $f^k - n^k M_{u^k,\Theta^k} = \mathscr{O}(\varepsilon)$, for $k \geq 1$, which confirms the relaxation effects we conjectured on the formal grounds and the AP ability of the scheme. In particular, the scheme does not encounter stability difficulties for small ε's; it still works perfectly under stability conditions determined only by the convection terms.

4.4 Temperature dependent viscosity

It makes sense to consider the case where the viscosity μ depends on the temperature of the flows. In particular, Sutherland [47] proposed the following formula

$$\mu = \mu_0 \left(\frac{\Theta}{\Theta_0}\right)^{3/2} \frac{\Theta_0 + S}{\Theta + S}$$

where μ_0 is a reference viscosity, Θ_0 is a reference temperature, and S is an effective temperature, called the Sutherland constant, which is characteristic of the considered fluid. Accordingly, the Fokker–Planck term $\frac{1}{\varepsilon} L_{u,\Theta} f$ is replaced by $\frac{\mu(\Theta)}{\varepsilon} L_{u,\Theta} f$. For the sake of simplicity we take $\mu_0 = 1$, $T_0 = 1$, and $S = 0.5$. If the stiff term is treated fully implicitly, one is led to a nonlinear system involving $\mu(\Theta^{n+1})$ for determining the hydrodynamic quantities in the first step of the algorithm. A Newton's algorithm is needed, which can impact the performances of the code. We avoid this difficulty by using a semi-implicit formulae where the viscosity is set to $\mu(\Theta^n)$ instead.

We work with the following initial data

$$\begin{array}{lll} \rho(0,x) = 1, & u(0,x) = 0, & \Theta(0,x) = 0.2 + 9\mathbf{1}_{[0.5,0.6]}\,, \\ n(0,x) = 1, & V(0,x) = 0, & \Theta_P(0,x) = 1\,, \end{array}$$

with $\varepsilon = 1$, $\gamma = 1.4$, $\rho_P/\rho_F = 5$, on the grid $N_x = 50$, $N_v = 32$. Figure 7 shows the profiles of the macroscopic variables at time $T = 0.2$. The red dots show the results derived by using the Sutherland viscosity, while the blue lines correspond to the constant viscosity case. The effect of this modification is sensible on the evolution of the temperatures: it seems that the energy exchange is stronger with Sutherland's viscosity. The particles get more energy from the fluid.

4.5 Effects of the state law and different kinetic approximations

We finally check the ability of the scheme in dealing with general $\gamma-$state laws. As detailed above it modifies the expression of the numerical fluxes for hydrodynamics, as defined by the kinetic scheme. We take $\rho_P/\rho_F = 5$, $\varepsilon = 0.1$. The initial data are taken as in (18) and (19). The results at $t = 20$ are shown in Figure 8. The qualitative behavior of the solutions is not significantly changed. Note in particular we do not observe the variety of shapes for large time asymptotics as it occurs in the isentropic case, see [12, 13]: all solutions seem to have the same stationary solution as asymptotic profile. On the same token, we mention that the choice of the equilibrium to be used in the definition of the kinetic scheme does not influence the simulation, at least in the situations we have tried.

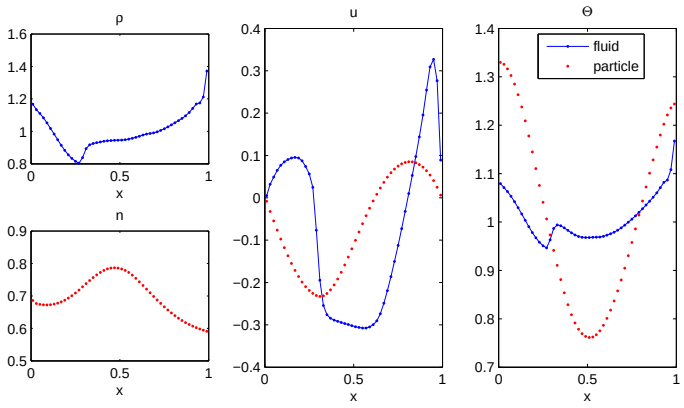

(a) $\varepsilon = 1$

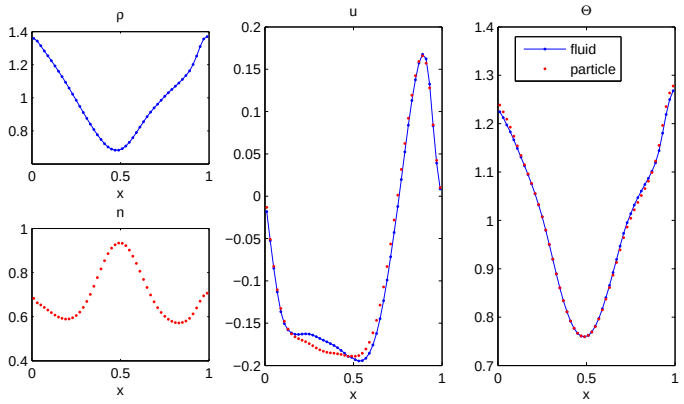

(b) $\varepsilon = 10^{-2}$

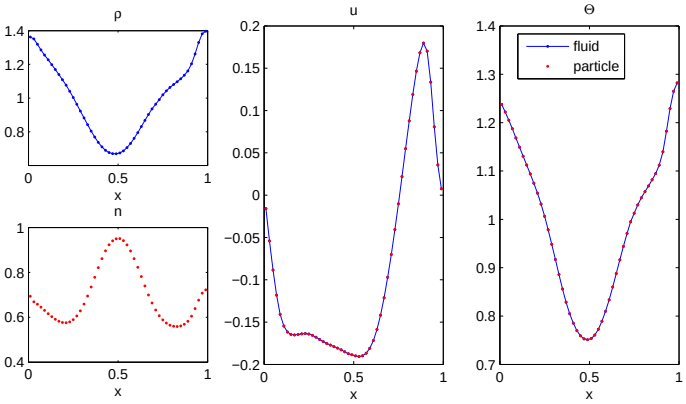

(c) $\varepsilon = 10^{-4}$

Figure 5: Macroscopic profiles for the fluid (up) and the particles (down) at $T = 0.3$, with different ε. Here $\gamma = 1.4$, $\frac{\rho_P}{\rho_F} = 2$.

Conclusion

We have introduced a new numerical scheme for simulating a system coupling the Vlasov–Fokker–Planck equation to the Euler system through drag force, momentum and energy exchanges. In

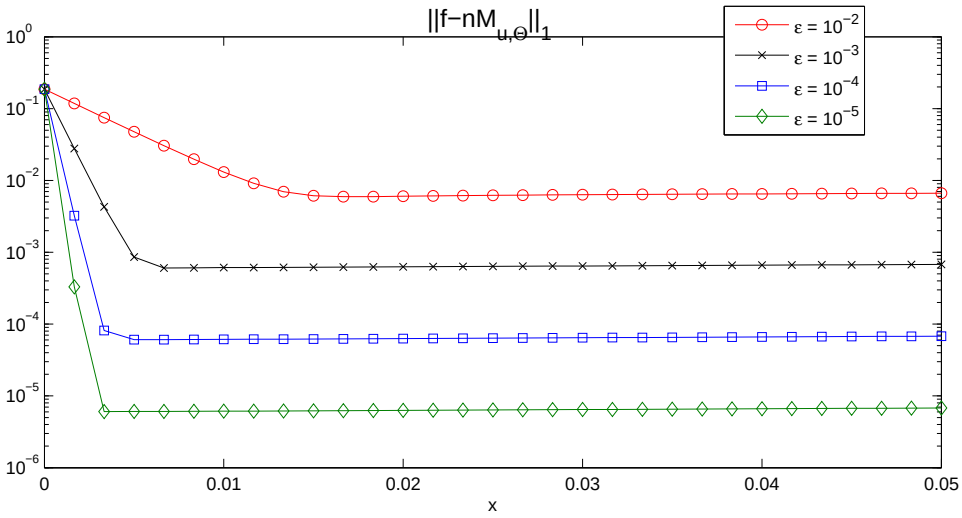

Figure 6: The L^1 distance between $f(t,x,v)$ and the equilibrium $n(t,x)M_{u(t,x),\Theta(t,x)}(v)$, with different ε. Here $\gamma = 1.4$, $\frac{\rho_P}{\rho_F} = 2$, $N_x = 50$, $N_v = 32$.

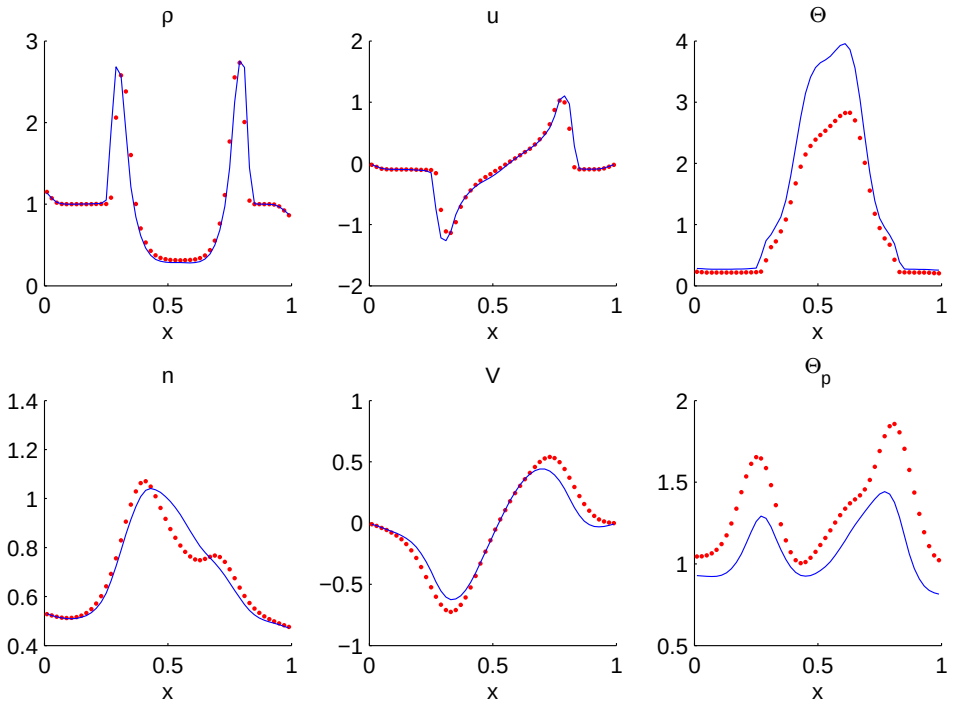

Figure 7: Macroscopic profiles for the fluid (up) and the particles (down) at $T = 0.2$, with constant viscosity (blue lines) and Sutherland's viscosity (red dots). Here $\gamma = 1.4$, $\varepsilon = 1$, $\rho_P/\rho_F = 5$.

particular the scheme is Asymptotic Preserving in the regime of small Stokes numbers which drives the system towards a set of purely hydrodynamic equations. The method is based on the implicit

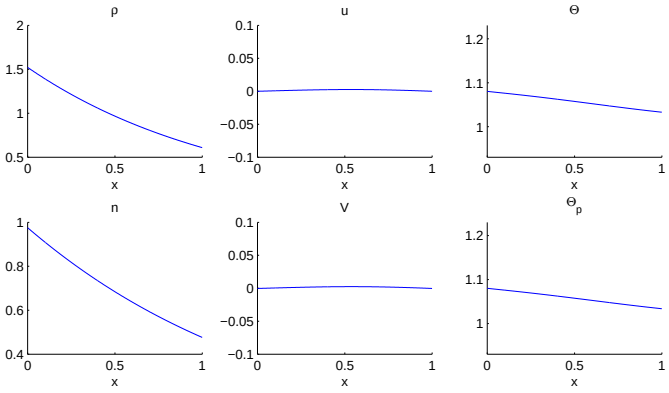

(a) $\gamma = 1.4$

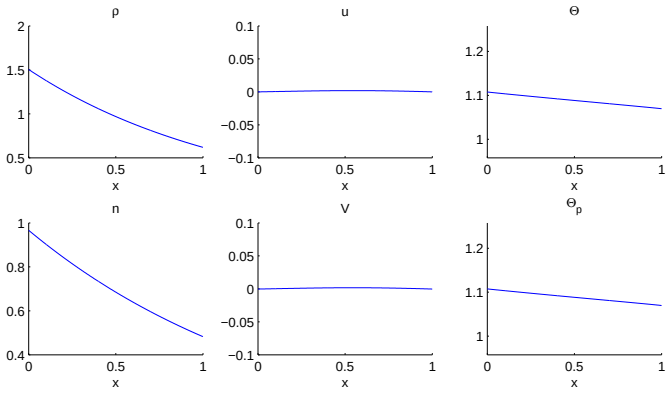

(b) $\gamma = 2$

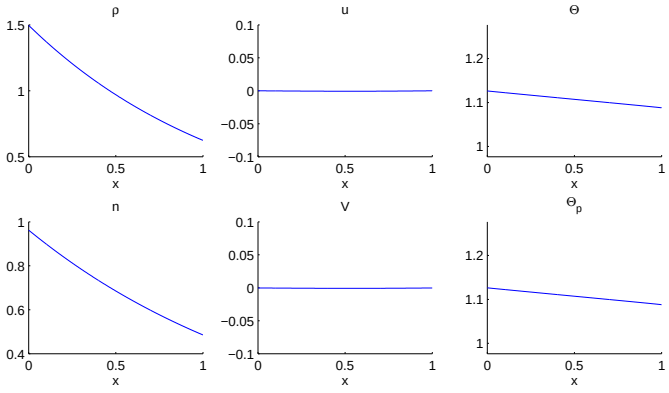

(c) $\gamma = 3$

Figure 8: Macroscopic profiles for the fluid (up) and the particles (down) at $T = 20$, with different γ. Here $\varepsilon = 0.1$, $\frac{\rho_P}{\rho_F} = 5$, $N_x = 1000$, $N_v = 32$.

treatment of the potentially stiff terms and relies on the possibility of updating the macroscopic unknowns by solving simple linear systems. The use of a kinetic scheme for solving the hydrodynamic

equations turns out to be very appropriate because the scheme for the complete problem becomes naturally an extended kinetic scheme for the limit system as the scaling parameter becomes small. Based on numerical evidence, the scheme also exhibits mass conservation, entropy dissipation, and up to mesh dependent error terms, energy conservation and well-balanced property. Furthermore the scheme can easily incorporate relevant generalizations of the basic model like considering general state law, or temperature–dependent viscosities.

Acknowledgements

This work started with a visit of Thierry Goudon at the Math. Department of UW-Madison. Thanks are addressed for the warm hospitality of the Department.

Shi Jin's research was partially supported by NSF grant No. DMS-0608720, NSF FRG grant DMS-0757285, a Van Vleck Distinguished Research Prize and a Vilas Associate Award from University of Wisconsin-Madison.

References

[1] D. Aregba-Driollet and V. Milisik. Kinetic approximation of a boundary value problem for conservation laws. *Numer. Math.*, 97:595–633, 2004.

[2] C. Baranger, L. Boudin, P.-E. Jabin, and S. Mancini. A modeling of biospray for the upper airways. *ESAIM:Proc*, 14:41–47, 2005.

[3] C. Baranger and L. Desvillettes. Coupling Euler and Vlasov equations in the context of sprays: local smooth solutions. *Journal of Hyperbolic Differential Equations*, 3(1):1–26, 2006.

[4] S. Berres, R. Bürger, and E. M. Tory. Mathematical model and numerical simulation of the liquid fluidization of polydisperse solid particle mixtures. *Comput. Visual Sci.*, 6:67–74, 2004.

[5] L. Boudin, B. Boutin, B. Fornet, T. Goudon, P. Lafitte, F. Lagoutière, and B. Merlet. Fluid-particles flows: A thin spray model with energy exchanges. *ESAIM: Proc.*, 28:195–210, 2009.

[6] L. Boudin, L. Desvillettes, C. Grandmont, and A. Moussa. Global existence of solutions for the coupled Vlasov and Navier-Stokes equations. *Differential and Integral Equations*, 22(11–12), 2009.

[7] B. Boutin and P. Lafitte. Splitting schemes for fluid-particles flows with energy exchanges. Work in progress.

[8] R. Bürger, W. L. Wendland, and F. Concha. Model equations for gravitational sedimentation-consolidation processes. *Z. Angew. Math. Mech.*, 80(2):79–92, 2000.

[9] R. Caflisch. The fluid dynamic limit of the nonlinear Boltzmann equation. *Comm. Pure Appl. Math.*, 33(5):651–666, 1980.

[10] R. Caflisch and G. Papanicolaou. Dynamic theory of suspensions with Brownian effects. *SIAM J. Appl. Math.*, 43:885–906, 1983.

[11] J. A. Carrillo, R. Duan, and A. Moussa. Global classical solutions close to equilibrium to the Vlasov-Euler-Fokker-Planck system. Technical report, UABarcelona, 2010. Preprint.

[12] J. A. Carrillo and T. Goudon. Stability and asymptotics analysis of a fluid-particles interaction model. *Comm. PDE*, 31:1349–1379, 2006.

[13] J. A Carrillo, T. Goudon, and P. Lafitte. Simulation of fluid & particles flows: Asymptotic preserving schemes for bubbling and flowing regimes. *J. Comput. Phys.*, 227(16):7929–7951, 2008.

[14] J.-A. Carrillo, T. Karpery, and K. Trivisa. On the dynamics of a fluid-particle interaction model: The bubbling regime. Technical report, UABarcelona, 2010. Preprint.

[15] F. Coron and B. Perthame. Numerical passage from kinetic to fluid equations. *SIAM J. Numer. Anal.*, 28:26–42, 1991.

[16] S. M. Deshpande. Kinetic theory based new upwind methods for inviscid compressible flows. In *AIAA 24th Aerospace Science Meeting, Jan 6-9, 1986, Nevada, USA*, 1986. AIAA paper 86-0275.

[17] S. M. Deshpande. On the maxwellian distribution, symmetric form and entropy conservation for the euler equations. Technical report, NASA Langley Research Centre, Hampton, VA, 1986. NASA TP2613.

[18] B. Després and F. Lagoutière. Contact discontinuity capturing schemes for linear advection and compressible gas dynamics. *J. Sci. Comput.*, 16(4):479–524, 2002.

[19] L. Desvillettes. Some new results of existence for the theory of sprays. `http://www.newton.ac.uk/programmes/KIT/seminars/090710001.html`, 2010. Workshop "Fluid-Kinetic Modelling in Biology, Physics and Engineering", Isaac Newton Institute for Mathematical Sciences, Programme on PDEs in Kinetic Theories.

[20] A. Einstein. On the motion of small particles suspended in liquids at rest required by the molecular-kinetic theory of heat. *Ann. Physik*, 17:549–560, 1905.

[21] A. Einstein. Eine neue bestimmung der moleküldimensionen. *Ann. Physik*, 19:289–306, 1906. Doctoral dissertation, Zurich, 1905.

[22] T Elperin, N. Kleeorin, M. A Liberman, V. S L'vov, A. Pomyalov, and I Rogachevskii. Clustering of fuel droplets and quality of spray in Diesel engines. 2003. `http://arxiv.org/nlin.CD/0305017v1`.

[23] G. Falkovich, A. Fouxon, and M. G. Stepanov. Acceleration of rain initiation by cloud turbulence. *Nature*, 219:151–154, 2002.

[24] F. Filbet and S. Jin. A class of asymptotic–preserving schemes for kinetic equations and related problems with stiff sources. *J. Comp. Phys.*, 229(20):7625–7648, 2010.

[25] E. Godlewski and P.-A. Raviart. *Numerical approximation of hyperbolic systems of conservation laws*, volume 118 of *Appl. Math. Sc.* Springer, 1996.

[26] T. Goudon, P.-E. Jabin, and A. Vasseur. Hydrodynamic limit for the Vlasov-Navier-Stokes equations. I. Light particles regime. *Indiana Univ. Math. J.*, 53(6):1495–1515, 2004.

[27] T. Goudon, P.-E. Jabin, and A. Vasseur. Hydrodynamic limit for the Vlasov-Navier-Stokes equations. II. Fine particles regime. *Indiana Univ. Math. J.*, 53(6):1517–1536, 2004.

[28] T. Goudon, A. Moussa, L. He, and P. Zhang. The Navier–Stokes–Vlasov–Fokker–Planck system near equilibrium. *SIAM J. Math. Anal.*, 42(5):2177–2202, 2010.

[29] K. Hamdache. Global existence and large time behaviour of solutions for the Vlasov-Stokes equations. *Japan J. Indust. Appl. Math.*, 15:51–74, 1998.

[30] M. Ishii and T. Hibiki. *Thermo–fluid dynamics of two–phase flows.* Springer, 2011. 2nd edition.

[31] S. Jin. Efficient asymptotic–preserving (AP) schemes for some multiscale kinetic equations. *SIAM J. Sci. Comput.*, 21(2):441–454, 1999.

[32] S. Jin and B. Yan. An AP scheme for the Fokker–Planck–Landau equation. Technical report, Math. Dept., UW Madison, 2010.

[33] F. Lagoutière. A non-dissipative entropic scheme for convex scalar equations via discontinuous cell-reconstruction. *C. R. Math. Acad. Sci. Paris*, 338(7):549–554, 2004.

[34] F. Lagoutière. Non-dissipative entropy satisfying discontinuous reconstruction schemes for hyperbolic conservation laws. Technical report, Univ. Paris–Sud, 2010.

[35] G. Lavergne. *Modélisation de l'écoulement multiphasique dans le propulseur à poudre P230 d'Ariane 5*, 2004. Lecture Notes of the School of the Groupement Français de Combustion, Ile d'Oléron.

[36] J. Mathiaud. *Etude de systèmes de type gaz-particules.* PhD thesis, ENS Cachan, 2006.

[37] A. Mellet and A. Vasseur. Global weak solutions for a Vlasov-Fokker-Planck/Navier-Stokes system of equations. *Math. Mod. Meth. Appl. Sci*, 17(7):1039–1063, 2007.

[38] A. Mellet and A. Vasseur. Asymptotic analysis for a Vlasov–Fokker–Planck/compressible Navier–Stokes system of equations. *Comm. Math. Phys.*, 281(3):573–596, 2008.

[39] A. Moussa. *Etude mathématique et numérique du transport d'aérosols dans le poumon humain.* PhD thesis, ENS Cachan, 2009.

[40] P. J. O'Rourke. *Collective Drop Effects on Vaporizing Liquid Sprays.* PhD thesis, Princeton Univ., 1981. Available as Technical Report #87545 Los Alamos National Laboratory.

[41] M. Pelanti and R. LeVeque. High resolution finite volume schemes for dusty gas jets and plumes. *SIAM J. Sci. Comput.*, 28(4):1335–1360, 2006.

[42] B. Perthame. Second order Boltzmann schemes for compressible Euler equations in one and two space dimension. *SIAM J. Numer. Anal.*, 29(1):1–19, 1992.

[43] B. Perthame. *Kinetic formulation of conservation laws.* Oxford Lecture Series in Math. and its Appl. Oxford University Press, 2003.

[44] D. I. Pullin. Direct simulation methods for compressible gas flow. *J. Comput. Phys.*, 34:231–244, 1980.

[45] L. Saint-Raymond. *Hydrodynamic limits of the Boltzmann equation*, volume 1971 of *Lecture Notes in Math.* Springer, 2009.

[46] B. Sportisse. *Modélisation et simulation de la pollution atmosphérique.* PhD thesis, Université Pierre et Marie Curie, 2007. Habilitation à Diriger les Recherches, Sciences de l'Univers.

[47] W. Sutherland. The viscosity of gases and molecular force. *Philosophical Magazine*, S. 5(36):507–531, 1893.

[48] I. Vinkovic. *Dispersion et mélange turbulents de particules solides et de gouttelettes par une simulation des grandes échelles et une modélisation stochastique lagrangienne. Application à la pollution de l'atmosphère.* PhD thesis, Ecole Centrale de Lyon, 2005.

[49] F. A. Williams. *Combustion theory.* Benjamin Cummings Publ., 1985. (2nd edition).